

Role of spin-lattice coupling in the ultrafast demagnetization of $Gd_{1-x}Tb_x$ alloysA. Eschenlohr,^{1,2,*} M. Sultan,^{1,*†} A. Melnikov,³ N. Berggaard,^{1,‡} J. Wieczorek,¹ T. Kachel,²
C. Stamm,^{2,§} and U. Bovensiepen^{1,||}¹*Fakultät für Physik and Center for Nanointegration (CENIDE), Universität Duisburg-Essen, Lotharstrasse 1, 47048 Duisburg, Germany*²*Institut für Methoden und Instrumentierung der Forschung mit Synchrotronstrahlung, Helmholtz-Zentrum Berlin für Materialien und Energie GmbH, Albert-Einstein-Strasse 15, 12489 Berlin, Germany*³*Abteilung für Physikalische Chemie, Fritz-Haber-Institut der Max-Planck Gesellschaft, Faradayweg 4-6, 14195 Berlin, Germany*

(Received 10 December 2013; revised manuscript received 11 April 2014; published 27 June 2014)

After excitation by femtosecond laser pulses, Gd and Tb exhibit ultrafast demagnetization in two steps, with the time constant of the second step linked to the coupling strength of the $4f$ magnetic moments to the lattice. In time-resolved magneto-optical Kerr effect measurements of $Gd_{1-x}Tb_x$ alloys, we observe a decrease in this time constant from 33 to 9 ps with Tb content x increasing from 0 to 0.7. We explain this behavior by the stronger spin-lattice coupling of Tb compared to Gd, which increases the effective spin-lattice coupling in $Gd_{1-x}Tb_x$ with x . In contrast, the faster time constant of the first demagnetization step exhibits no dependence on x . Additional time- and element-resolved x-ray magnetic circular dichroism measurements show a two-step demagnetization of Gd and Tb in $Gd_{0.6}Tb_{0.4}$ with an equivalent time scale of the second step but a different magnitude of demagnetization which persists for 15 ps. We explain this by an increased coupling of the Gd $4f$ magnetic moments to the lattice compared to pure Gd, via interatomic exchange coupling to the neighboring Tb $4f$ moments mediated by $5d$ electrons, which has limited efficiency and allows an estimation of a characteristic time scale of the interatomic exchange coupling. We assign the first demagnetization step to the dynamics of the laser-excited $5d$ electrons, while the second demagnetization step is dominated by the strength of spin-lattice coupling of the $4f$ electrons.

DOI: [10.1103/PhysRevB.89.214423](https://doi.org/10.1103/PhysRevB.89.214423)

PACS number(s): 75.50.Cc, 75.78.Jp, 75.30.Et

I. INTRODUCTION

Ultrafast demagnetization of ferromagnetic metals after femtosecond laser excitation, which was first observed in 1996 [1], is an intriguing phenomenon which has only been incompletely understood so far, despite a large body of experimental and theoretical work on the subject (see [2,3] and references therein). The central question here is how spin angular momentum can be transferred in such an ultrafast way, and to which reservoir. An obvious candidate would be spin-lattice coupling, which, however, has been found to occur on a much slower time scale on the order of tens to hundreds of picoseconds [4,5]. Consequently, the microscopic origin of subpicosecond demagnetization is currently under debate. Spin-flip scattering processes such as an Elliott-Yafet type of electron-phonon scattering [6], electron-magnon [7], and electron-electron scattering [8,9] have been proposed, as well as ultrafast magnon emission [10]. Recent work also indicates the importance of spin transport in the superdiffusive regime for ultrafast demagnetization [11–15].

In order to find the relation between ultrafast demagnetization and the microscopic properties of magnetic materials relevant for a theoretical description thereof, such as

atomic magnetic moment and exchange coupling strength, the ability to vary these properties systematically can give valuable information. Here we investigate the effect of such variations by alloying Gd and Tb as two ferromagnetic elements. Several recent studies of ultrafast magnetization dynamics have been performed on magnetic materials consisting of more than one element, i.e. ferri- and ferromagnetic alloys. $Gd_{25}Fe_{65.6}Co_{9.4}$ showed decoupled dynamics of the Gd and Fe sublattices during ultrafast magnetization reversal and a transient ferromagnetic alignment of the initially antiferromagnetically coupled sublattices [16]. Such a transient ferromagnetic alignment has recently also been seen in ferrimagnetic $Tb_{16}Fe_{75}Co_9$ [17]. In $Ni_{80}Fe_{20}$, a delay in the demagnetization of Ni compared to Fe has been observed, which was increased by admixture of Cu [18].

In this article we focus on the coupling between the spin and lattice degrees of freedom via the orbital anisotropy, which plays a central role in the description of angular momentum transfer between the magnetization and the lattice. We aim to investigate the relation between spin-lattice coupling and ultrafast demagnetization by employing rare earth $Gd_{1-x}Tb_x$ alloys as a model system. In our recent study [19], we clarified the role of spin-lattice coupling in ultrafast magnetization dynamics of pure rare earths: In Gd and Tb, a two-step demagnetization was observed experimentally, in which an initial subpicosecond demagnetization with a time constant of 750 fs for both Gd and Tb was followed by a second, slower reduction of the magnetization. The first demagnetization step occurs on a nonequilibrium time scale, before equilibration between electrons and lattice has taken place [20]. A complex nonequilibrium response of the exchange-split band structure of pure Gd was observed recently on the same time scale [21]. Only the time constant of the second

*Both authors contributed to this work by comparable experimental efforts.

†Present address: Nanoscience Department, National Centre for Physics, Islamabad, Pakistan.

‡Present address: IPCMS, 23 rue du Loess, BP 43, 67034 Strasbourg Cedex 2, France.

§Present address: Department of Materials, ETH Zurich, CH-8093 Zurich, Switzerland.

||uwe.bovensiepen@uni-due.de

step, corresponding to quasiequilibrium demagnetization after electron-phonon equilibration, was found to be linked to the strength of spin-lattice coupling in the respective rare earth, which depends on the anisotropy of the $4f$ orbitals. In Tb, a time constant of 8 ps agrees with the strong spin-lattice coupling originating from the anisotropic orbital configuration for an orbital moment of $L = 3$ due to the $4f^8$ electron configuration. Gd demagnetized with a time constant of 40 ps, which we explained by the weaker spin-lattice coupling due to the $4f^7$ electron configuration resulting in $L = 0$ [22]. In rare earth compounds, long range magnetic order arises from indirect exchange coupling of the $4f$ electrons, which carry the largest part of the atomic magnetic moment, via the $5d$ electrons, i.e., RKKY coupling [23]. This coupling is rather strong, which is corroborated by a concomitant demagnetization of $4f$ and $5d$ magnetic moment contributions in Gd [24]. Note that the remaining weak spin-lattice coupling in Gd is also mediated by the $5d$ electrons [25]. In Tb atoms with an orbital quantum number of $L = 3$, the $4f$ magnetic moments exhibit considerably stronger coupling to the lattice than the $4f$ moments of Gd ($L = 0$), which can only couple indirectly via the $5d$ electrons, as discussed above and shown schematically in Fig. 1(b). By alloying Gd and Tb we thus continuously modify the effective strength of spin-lattice coupling according to the alloy composition while staying in an ordered ferromagnetic phase, as will be discussed below.

Here we report on complementary experiments employing the time-resolved magneto-optical Kerr effect (MOKE) in the visible wavelength range and time- and element-resolved x-ray magnetic circular dichroism (XMCD) measurements on $Gd_{1-x}Tb_x$ alloys. MOKE allows us to probe concentration dependent magnetization dynamics of the $5d$ electrons [compare Fig. 1(a)] over a wide range of alloy compositions. We find a continuous decrease of the time constant of the second demagnetization step from 33 to 9 ps with the Tb content increasing from 0 to 0.7, which we assign to a spin-lattice coupling increasing with the Tb fraction. In contrast, the time constant of the first demagnetization step is found to

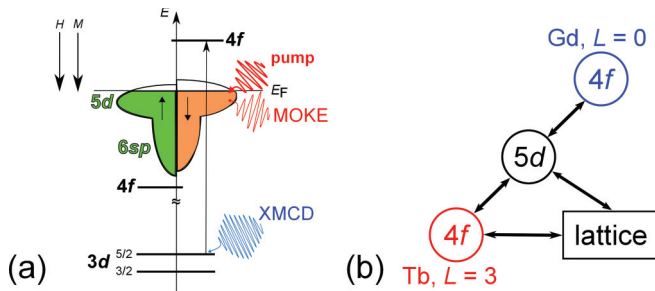


FIG. 1. (Color online) (a) Schematic electronic density of states for rare earth elements Gd and Tb. 1.5 eV pump pulses excite predominantly $5d$ electrons in the vicinity of the Fermi level E_F , which are probed by time-resolved MOKE at the same photon energy. XMCD at the M_5 -edge probes the $4f$ magnetic moments directly and element selectively by resonantly exciting the $3d_{5/2}$ core level electrons to the unoccupied $4f_{\downarrow}$ states. \uparrow and \downarrow denote majority and minority spins, while H and M refer to the external magnetic field and magnetization, respectively. (b) The coupling between Gd and Tb $4f$ and $5d$ magnetic moments and the lattice in $Gd_{1-x}Tb_x$ alloy is shown schematically.

be uncorrelated to the amount of Tb in the alloy. With XMCD, we distinguish the dynamics of the Gd and Tb $4f$ magnetic moments by employing a resonant core level excitation at the M_5 edges as a probe [see Fig. 1(a)]. With this element-selective probe we find a shared slower time constant of the Gd and Tb $4f$ moments in $Gd_{0.6}Tb_{0.4}$. Thus, the second step of demagnetization of Gd in the alloy is accelerated compared to pure Gd. Therefore, the Gd $4f$ magnetic moments in the GdTb alloy experience a stronger coupling to the lattice compared to the pure metal. We estimate the angular momentum transfer from the $4f$ shell to the lattice, and between Gd and Tb in the alloy with a rate model, which allows us to attribute a transiently different magnitude of demagnetization between Gd and Tb to a limited efficiency of interatomic exchange coupling mediated by the $5d$ electrons.

II. EXPERIMENTAL RESULTS

A. Concentration dependence of ultrafast demagnetization

The magneto-optical Kerr effect (MOKE) has been used to investigate the concentration dependence of the ultrafast demagnetization of $Gd_{1-x}Tb_x$ thin films for a Tb content x of $0 \leq x \leq 0.7$. Static and time-resolved MOKE measurements were performed at 790 nm wavelength in longitudinal configuration, i.e., with an external magnetic field oriented in the sample plane and parallel to the plane of incidence of the laser beam.

Epitaxial, 20 nm thick $Gd_{1-x}Tb_x$ films with (0001) orientation were prepared in ultrahigh vacuum at a base pressure $< 10^{-10}$ mbar by coevaporation from electron beam-heated Gd and Tb sources on W(110) at room temperature. After deposition, the samples were annealed at 700 K for 10 min to get smooth epitaxial films. The static magnetic properties of our samples were analyzed by hysteresis loops at base temperatures of 220 K or higher, as at these temperatures the sample's magnetization could be reversed with the magnetic field of a maximum 0.05 T available in the experimental chamber [compare Fig. 2(a)]. In Fig. 2(b) the change in magnetization with temperature, as measured by the Kerr rotation, is displayed. The Curie temperature T_C was estimated from the point where the normalized magnetization M/M_0 is about to vanish. As can be seen in the inset of Fig. 2(b), the resulting values of T_C of the GdTb alloys decrease linearly with increasing Tb content from 293 K for pure Gd to 250 K for $Gd_{0.3}Tb_{0.7}$, in accordance with literature [23]. The existence of a well-defined T_C demonstrates that our samples are homogeneous ferromagnetic alloys. Furthermore, the change in the shape of the hysteresis loops, going from rectangular for pure Gd to more hard axis like for high Tb content, see Fig. 2(a), originates from the in-plane magnetic anisotropy introduced by Tb: The W(110) substrate was oriented in such a way that the easy axis of the rare earth film was set perpendicular to the optical plane. This means that in the longitudinal geometry used here the external magnetic field is applied along the hard axis. For pure Gd with no in-plane magnetic anisotropy the axes parallel and perpendicular to the optical plane are equivalent and the sample surface is thus an easy plane. With increasing x , the anisotropy of $Gd_{1-x}Tb_x$ grows, changing the shape of the hysteresis loops. The hysteresis loops in Fig. 2(a) also show an increased coercivity for alloys with higher Tb

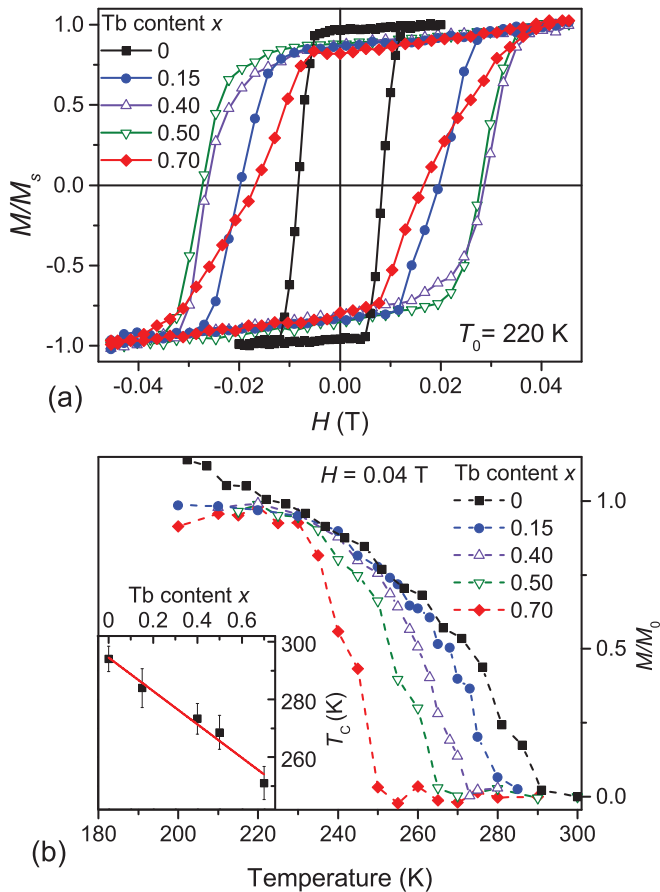


FIG. 2. (Color online) Characterization of the magnetic properties of epitaxial $\text{Gd}_{1-x}\text{Tb}_x$ films on W(110) by static MOKE. (a) Magnetization M , normalized to the saturation magnetization M_s , depending on the external magnetic field H , measured at a base temperature T_0 of 220 K. Increasing coercivity and/or changing shape of the hysteresis loops with increasing Tb content point to the influence of the strong Tb spin-lattice coupling. (b) Temperature-dependent magnetization M , normalized to its value M_0 at 220 K. The inset shows the linear concentration dependence of the Curie temperature T_c . The line is a guide to the eye.

content up to $x = 0.5$. This effect is consistent with the higher magnetocrystalline anisotropy of Tb, caused by the stronger spin-lattice coupling of its $4f$ magnetic moments compared to Gd [26]. These static measurements indicate a stronger effective spin-lattice coupling of $\text{Gd}_{1-x}\text{Tb}_x$ with increasing Tb content. Next, we investigate how the concentration-dependent modification of the spin-lattice coupling affects the magnetization dynamics of the GdTb alloys.

Femtosecond time-resolved pump-probe experiments were performed using a cavity-dumped Ti:sapphire oscillator with a central wavelength of 790 nm, generating 35 fs pulses at a repetition rate of 1.52 MHz. For both the pump and probe beams the fundamental wavelength was employed, with a pump-probe intensity ratio of 4:1. Pump and probe beams impinge on the sample almost collinearly, at an angle of about 45° with respect to the sample normal. All time-resolved MOKE measurements shown in the following were performed at an absorbed pump laser fluence of 1 mJ/cm^2 . The base temperature was set to 220 K, which was required to ensure

magnetization reversal of the epitaxial film with its high magnetic anisotropy energy due to the Tb constituent [27]. The Kerr rotation was determined by polarization analysis of the reflected probe beam via a Wollaston prism and a balanced diode scheme. To obtain the MOKE signal, the external magnetic field of 0.04 T was reversed at each point in the pump-probe delay scan, thus reversing the sample's magnetization. The difference between the signals for opposite magnetization directions measured in closed and open phase of the chopper placed in the pump beam, gives the Kerr rotation of the probe beam polarization θ_0 and θ before and after excitation, respectively, which is proportional to the transient magnetization. To exclude errors in the detector calibration, we use the normalized quantity $\Delta\theta/\theta_0 = \theta/\theta_0 - 1$ to characterize relative pump-induced variations of the magnetization.

The results of our time-resolved MOKE analysis for different compositions of $\text{Gd}_{1-x}\text{Tb}_x$ are displayed in Fig. 3(a). For all compositions, the transient Kerr rotation shows an ultrafast drop of the magnetization within the first few picoseconds after laser excitation, followed by a second, slower magnetization reduction before the magnetization recovers back to its initial value on the time scale of a few hundred picoseconds. Thus, demagnetization of GdTb alloys occurs on two distinct time scales as observed in thin polycrystalline Gd and Tb films [19] and epitaxially grown Gd on W(110) [28]. The demagnetization curves of $\text{Gd}_{1-x}\text{Tb}_x$ change strongly with increasing Tb content. The change of magnetization, proportional to $\Delta\theta/\theta_0$, reached after about 200 ps, i.e., after equilibration of the spin system and the lattice, is getting larger with x . This can be explained in terms of the static temperature-dependent behavior of the magnetization, which is reasonable at this delay: Since T_c of $\text{Gd}_{1-x}\text{Tb}_x$ is reduced with increasing x [compare Fig. 2(b)], bringing the same amount of energy into the ferromagnetic layer by pumping with the same laser fluence and starting at the same base temperature, will, after thermal equilibration, lead to heating increasingly closer to T_c , and thus a stronger demagnetization. Afterwards, recovery of the magnetization back to its value before laser excitation occurs on the time scale of heat dissipation out of the ferromagnetic film into the substrate. More importantly, the maximum amount of demagnetization is reached faster for alloys with a higher Tb content, meaning that the second magnetization drop is accelerated with increasing Tb content.

In order to quantify this dynamics, we determine the corresponding time constants of demagnetization by fitting the time-dependent MOKE data from Fig. 3(a) with a double exponential decay of the form

$$\frac{\Delta\theta(t)}{\theta_0} = S(t) \left[C_0 + \frac{\Delta M_1}{M} (1 - e^{-t/\tau_1}) + \frac{\Delta M_2}{M} (1 - e^{-t/\tau_2}) \right], \quad (1)$$

where the indices 1 and 2 refer to the first and second step in the demagnetization, respectively, $\frac{\Delta M}{M}$ is the amplitude, τ is the time constant, and $S(t)$ is a step function at time zero. C_0 is introduced to describe a steplike change in the Kerr rotation during the first 150 fs observed previously [29]. In the present article we focus on the subsequent reduction of the magnetization. The resulting time constant τ_2 for the second magnetization decrease shows a strong change when

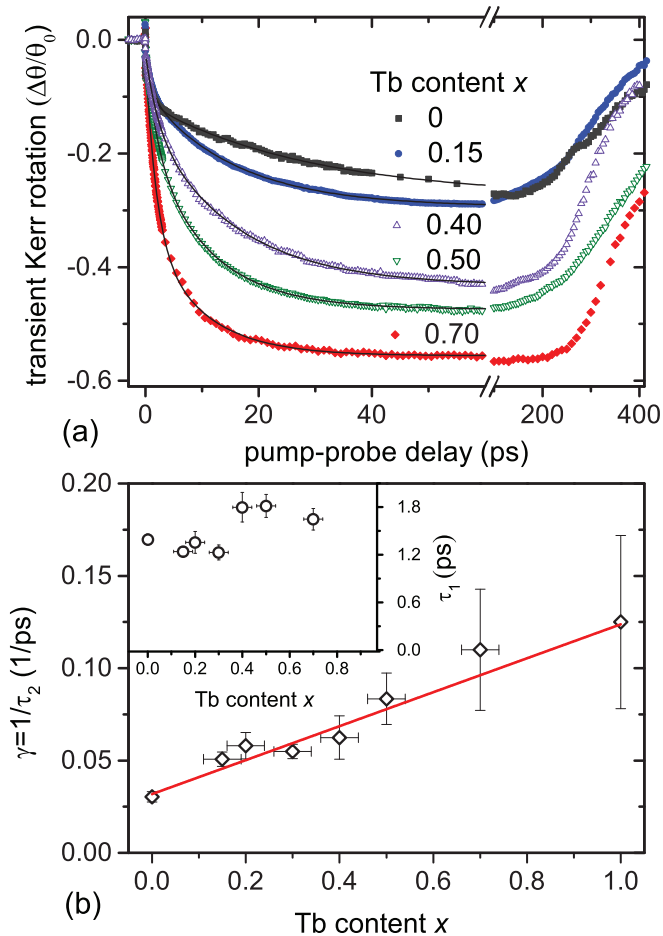


FIG. 3. (Color online) Dependence of ultrafast magnetization dynamics on the Tb concentration x in $\text{Gd}_{1-x}\text{Tb}_x$ alloy measured with time-resolved MOKE at a base temperature of 220 K and in an external magnetic field of ± 0.04 T. (a) The transient change of the magnetization, as measured by the change in Kerr rotation $\Delta\theta$ normalized to the value θ_0 for the unexcited sample, is displayed for five different Tb concentrations ranging from 0 (uppermost curve) to 0.7 (lowermost curve). (b) The resulting rate of the quasiequilibrium process $\gamma = 1/\tau_2$, with τ_2 being the time constant of the second step of demagnetization as derived from double exponential fits to the time-resolved MOKE data [plotted as black lines in (a)], shows an increase towards larger Tb concentration. This behavior is well described by a linear fit to the data (solid line). γ for pure Tb is taken from [19]. Inset: In the time constant τ_1 of the first step of demagnetization, no clear trend with increasing Tb concentration can be observed.

going from pure Gd to $\text{Gd}_{0.85}\text{Tb}_{0.15}$, from 33 to 20 ps, which indicates that the spin-lattice coupling of Tb dominates the magnetization dynamics in the alloys on longer time scales already for a rather low Tb content. Moreover, we see a continuous decrease in the time constant for the second demagnetization step when the Tb content is increased further. The rate of this quasiequilibrium process $\gamma = 1/\tau_2$ [see Fig. 3(b)] can be fitted with a linear dependence, including the value previously found for pure Tb and linked to its strong, direct $4f$ -lattice coupling [19]. We can thus attribute the accelerated demagnetization to an increased effective spin-lattice coupling in GdTb with increasing Tb content.

The time constants τ_1 of the first magnetization drop vary between 1.2 and 1.8 ps, as shown in the inset of Fig. 3(b). These time constants are larger than the time constant of about 750 fs observed previously on pure, epitaxially grown Gd [28] at a base temperature of 50 K. This difference in the time constants is due to the different base temperatures in [28] and the measurement presented here. A similar increase from about 800 fs to 1.2 ps when raising the temperature from 80 to 220 K has previously been observed on pure Gd and attributed to an increased contribution of phonon-mediated spin-flip scattering processes to ultrafast demagnetization when going above the Debye temperature [29]. Coming back to the concentration dependence in $\text{Gd}_{1-x}\text{Tb}_x$, τ_1 does not show any particular trend when the alloy composition is varied, in striking contrast to τ_2 . The fact that τ_2 exhibits a clear dependence on the spin-lattice coupling strength represents the main result of our concentration dependent time-resolved MOKE measurements.

The question remains whether only Tb in $\text{Gd}_{1-x}\text{Tb}_x$ contributes to the accelerated demagnetization for higher Tb content. The Gd and Tb $4f$ moments are coupled through the *interatomic* exchange mediated by $5d$ electrons and $4f$ - $5d$ *intra-atomic* coupling [see Fig. 1(b) and Sec. I]. It can thus be expected that also the Gd $4f$ moments in a GdTb alloy show an enhanced coupling to the lattice which is then mediated by the interatomic exchange coupling to neighboring Tb atoms. Element-sensitive XMCD measurements were therefore employed in order to disentangle the individual contributions of the Gd and Tb $4f$ magnetic moments in the alloy, which will be described in the next section.

B. Element-resolved ultrafast magnetization dynamics

X-ray magnetic circular dichroism (XMCD) is the difference of absorption of circularly polarized x rays in a ferromagnetic or ferrimagnetic sample for parallel and antiparallel alignment of the sample's magnetization with respect to the x-ray propagation direction [30]. Since XMCD involves an electronic transition from a core level to the unoccupied $4f_1$ states in Gd and Tb [compare Fig. 1(a)], it is an element-specific probe, which allows us to look at the elemental constituents of GdTb separately. With XMCD at the $M_{5,4}$ edges, we directly probe the localized $4f$ magnetic moments of Gd and Tb in the alloy and complement the magneto-optical analysis above. Static and time-resolved XMCD measurements were performed at the BESSY II storage ring operated by Helmholtz Zentrum Berlin für Materialien und Energie GmbH, Berlin, Germany.

For XMCD measurements in transmission geometry, 10 nm thick polycrystalline $\text{Gd}_{0.6}\text{Tb}_{0.4}$ samples were prepared by co-evaporation from Gd and Tb sources on 500 nm thick freestanding Al foils under UHV conditions at a base pressure $< 10^{-10}$ mbar and at room temperature [31]. Y buffer and cap layers of 50 and 5 nm thickness, respectively, were employed to protect the rare earth film against degradation. The Gd and Tb $4f$ magnetic moments in the alloy show ferromagnetic alignment, as can be seen from the negative (positive) XMCD at both M_5 (M_4) absorption edges in the static XMCD spectra in Fig. 4. The base temperature for the XMCD analysis was set to 82 K, well below the Curie temperature of about 270 K for this alloy composition, see Fig. 2(b) and [23]. Furthermore, Gd and Tb exhibit identical hystereses in the alloy; an external

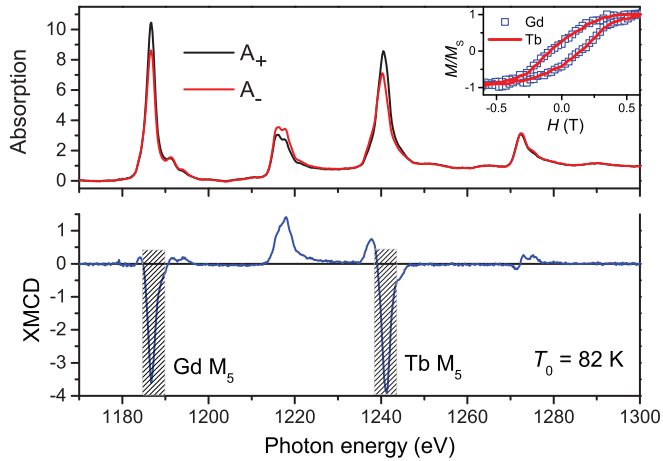


FIG. 4. (Color online) X-ray absorption spectra of $\text{Gd}_{0.6}\text{Tb}_{0.4}$ at the Gd and Tb $M_{5,4}$ edges measured with circularly polarized x rays, with the sample's magnetization oriented parallel (A_+) and antiparallel (A_-) to the x-ray propagation direction by applying an external magnetic field $H = \pm 0.5$ T, are displayed in the upper panel. The absorption spectra are normalized to the continuum step after the Tb M edges. The lower panel shows the XMCD, which is proportional to $A_- - A_+$, with the proportionality factor [32] given by the angle of 35° to the surface normal under which H is applied and the x-ray polarization degree of 90%. The shaded areas mark the photon energies where the time-resolved XMCD measurements were performed. The inset depicts element-resolved hysteresis loops of Gd and Tb, taken at the respective M_5 edges.

magnetic field of ± 0.5 T applied along the x-ray propagation direction is sufficient to saturate the sample's magnetization, as can be seen in the inset of Fig. 4. Since the magnetization of the $\text{Gd}_{0.6}\text{Tb}_{0.4}$ sample is oriented preferentially in plane [33], and XMCD measures the projection of the $4f$ magnetic moments along the x-ray propagation direction, the angle between the sample normal and the x-ray propagation direction was set to 35° for all static and time-resolved XMCD measurements.

For the time- and element-resolved measurements of the magnetization dynamics, the x-ray energy was fixed to the value for the maximum dichroic signal at the M_5 edge of Gd at 1186 eV, or respectively to 1241 eV for Tb. At each step in the pump-probe delay, the XMCD signal was obtained by reversing the external magnetic field applied to the sample. Circularly polarized, 100 fs short x-ray probe pulses were provided by the BESSY II Femtoslicing source [34,35]. In the Femtoslicing process, an intense femtosecond laser pulse modulates the energy of a part of an electron bunch circulating in the storage ring, allowing this ultrashort "slice" of electrons to be split off from the main bunch and radiate a correspondingly short x-ray pulse in a subsequent insertion device. At the BESSY II source, x rays are generated at a repetition rate of 6 kHz, provided by a first Ti:sapphire amplifier, while the pump pulses are generated from a second amplifier running at 3 kHz, seeded by the same Ti:sapphire oscillator. In the pump-probe measurements we thus alternate between pump-probe and probe only, leading to a high sensitivity towards pump-induced dynamics. For exciting the sample, 50 fs laser pulses with 780 nm wavelength and an incident fluence of 3.4 mJ/cm^2 were used. Due to the jitter-free synchronization of the laser

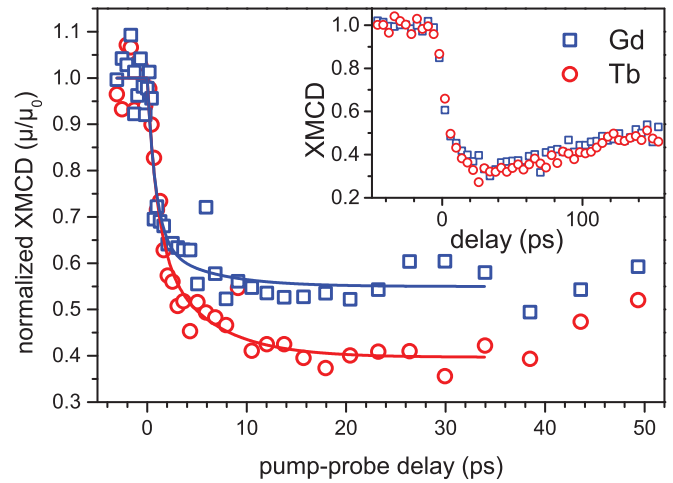


FIG. 5. (Color online) Time- and element-resolved ultrafast demagnetization of Gd (squares) and Tb (circles) in $\text{Gd}_{0.6}\text{Tb}_{0.4}$. The temporal evolution of the XMCD signal, which corresponds to the transient, element-resolved $4f$ magnetic moment μ , normalized to its value μ_0 before laser excitation, is shown for a pump-probe delay of up to 50 ps. XMCD acquired with 10 ps long x-ray pulses is displayed in the inset. All XMCD measurements were performed at base temperature 82 K and in an external magnetic field of ± 0.5 T.

pump pulses and x-ray probe pulses, which are generated from the same source, i.e., Ti:sapphire oscillator, this setup results in a total time resolution of 130 fs for the time-resolved XMCD measurements [35].

As can be seen in Fig. 5, a reduction of both the Gd and Tb $4f$ magnetic moments in the alloy is observed after laser excitation. The main figure shows data with 130 fs time resolution. For the inset, longer x-ray pulses with a duration of 10 ps full width at half maximum, which are provided in the low- α mode of the BESSY II storage ring [36], were employed. This dataset shows that the recovery of the magnetic moments of both constituents on a time scale of several hundred picoseconds proceeds simultaneously. The initial drop in the magnetic moments is broadened in time here due to the x-ray pulse duration of 10 ps [36] and potentially some additional electronic jitter between pump and probe which does not occur in Femtoslicing mode. The dataset with 130 fs time resolution reveals that the demagnetization happens in two steps, with the first, subpicosecond step comprising about half of the total magnitude of demagnetization. This initial drop results in a relative change of the magnetic moment μ/μ_0 of Gd and Tb, respectively, to about 0.7, where μ_0 represents the equilibrium value of the magnetic moment before optical excitation. Subsequently, the magnetic moment of Tb is reduced to about $0.4\mu_0$ during the next 20 ps, before recovery sets in at a longer time scale. The dynamic behavior of Gd in the alloy follows that of Tb. Interestingly, the magnitude of demagnetization is slightly lower than for Tb.

In order to analyze these experimental results in a more quantitative manner, the demagnetization curves were fitted with a double exponential decay of the form

$$\mu(t) = \mu_0 + S(t)[\Delta\mu_1(1 - e^{-t/\tau_1}) + \Delta\mu_2(1 - e^{-t/\tau_2})], \quad (2)$$

TABLE I. Overview of demagnetization time constants of pure Gd, Tb, and $\text{Gd}_{1-x}\text{Tb}_x$ alloy. The element-averaged time constants for $\text{Gd}_{0.6}\text{Tb}_{0.4}$ from our MOKE analysis are somewhat different from those found in our XMCD measurements due to the different base temperatures in these experiments, as discussed in the main text.

	τ_1 (ps)	τ_2 (ps)
Gd [4]	–	100 ± 80
Gd [41]	–	48
Gd [19]	0.76 ± 0.25	40 ± 10
Gd [28]	0.70	–
Gd [21]	0.86 ± 0.10	–
Gd in $\text{Gd}_{0.6}\text{Tb}_{0.4}$ (this work)	0.89 ± 0.29	5.3 ± 2.3
Tb in $\text{Gd}_{0.6}\text{Tb}_{0.4}$ (this work)	1.03 ± 0.25	5.3 ± 2.3
$\text{Gd}_{0.6}\text{Tb}_{0.4}$ (MOKE, this work)	1.80 ± 0.19	16 ± 3
Tb [19]	0.74 ± 0.25	8 ± 3

where $S(t)$ refers to a step function at time zero, μ_0 is the initial XMCD value at negative pump-probe delay, i.e., the magnetic moment under equilibrium conditions, and τ_i and $\Delta\mu_i$, $i = 1, 2$ are the time constant and amplitude of the first femtosecond and second picosecond exponential decay, respectively. In order to facilitate a comparison, we list the time constants τ_1 and τ_2 for pure Gd, Tb, and $\text{Gd}_{0.6}\text{Tb}_{0.4}$ as known from literature and this study in Table I. For the first step of demagnetization, the double exponential fit results in characteristic time constants of 0.89 ± 0.29 ps for Gd and 1.03 ± 0.25 ps for Tb in $\text{Gd}_{0.6}\text{Tb}_{0.4}$. These time constants agree within error bars with those found in pure Gd and Tb [19] (compare Table I). The time constants for $\text{Gd}_{0.6}\text{Tb}_{0.4}$ measured with XMCD are both shorter than the element-averaged one derived from our MOKE measurements for the same alloy composition, which is 1.8 ± 0.2 ps. This deviation is due to the different equilibrium temperatures for MOKE and XMCD measurements of 220 and 82 K discussed in [29] and above.

Regarding the second step of demagnetization, a common time constant of 5.3 ± 2.3 ps for Gd and Tb is obtained. The second step in the demagnetization of $\text{Gd}_{0.6}\text{Tb}_{0.4}$ thus occurs with a time constant that is slightly smaller [37] but comparable to that of pure Tb (8 ± 3 ps, compare Table I and [19]). Therefore, the demagnetization of Gd in GdTb alloy is clearly faster than that of pure Gd, which shows a time constant of 40 ± 10 ps [19] (see also Table I). Consequently, the accelerated demagnetization of Gd in $\text{Gd}_{60}\text{Tb}_{40}$ confirms an enhanced coupling of the Gd $4f$ magnetic moments to the lattice via $5d$ electron mediated interatomic exchange coupling to the neighboring Tb atoms, which represents the main result of our time- and element-resolved XMCD measurements.

The origin of the difference in the relative magnitude of demagnetization for Gd and Tb in $\text{Gd}_{0.6}\text{Tb}_{0.4}$ between 5 and 40 ps, see Fig. 5, remains to be discussed [38]. As will be discussed below, this difference is a consequence of the different spin-lattice coupling of Gd and Tb, cf. Fig. 1(b). It furthermore leads to an estimation of the characteristic time scale of the interatomic exchange coupling mediated by the $5d$ electrons and the respective magnetic moment transfer rate. The scheme of angular momentum transfer indicated in Fig. 1(b) already suggests that in a quasiequilibrium process the demagnetization of the Tb $4f$ shell must be stronger

than that of the Gd $4f$ shell to provide a significant flow of angular momentum from Gd $4f$ to Tb $4f$ through the $5d$ electrons. In this light, the observed smaller demagnetization of the Gd $4f$ shell appears to be reasonable. In the following we describe the angular momentum transfer processes during the second step of demagnetization in $\text{Gd}_{1-x}\text{Tb}_x$ with a simple rate model in order to account for our observations from the concentration-dependent and element-resolved experiments.

III. DISCUSSION

A. The characteristic time scale of the RKKY exchange interaction

In order to further narrow down the microscopic mechanisms behind the second demagnetization step observed in $\text{Gd}_{1-x}\text{Tb}_x$, we estimate the amount of angular momentum transferred between the localized $4f$ magnetic moments, the $5d$ electrons, and the collective excitations of the lattice [39], as shown schematically in Fig. 1(b). Here we expand on a similar estimate performed in our previous study on pure Gd and Tb [19] by now taking concentration dependent changes in $\text{Gd}_{1-x}\text{Tb}_x$, as well as angular momentum transfer between the Gd and Tb magnetic moments into account.

We first look at the element-averaged angular momentum transfer rate γ from the Gd and Tb magnetic moments to the lattice, which changes with the Tb concentration x , as seen in our time-resolved MOKE measurements [compare Fig. 3(b)]. In a quasiequilibrium demagnetization process, which is taking place on the second, slower demagnetization step observed here in $\text{Gd}_{1-x}\text{Tb}_x$, the change in magnetization with time is given at the beginning of this quasiequilibrium process by $dm/dt|_{t \approx 0} = -\gamma \cdot \Delta m$. Here Δm represents the relative change of magnetization within the second demagnetization step in units of the saturated moment $\mu_S = x\mu_{\text{Tb}}^0 + (1-x)\mu_{\text{Gd}}^0$, with $\mu_{\text{Tb}}^0 = 9.34 \mu_B$ and $\mu_{\text{Gd}}^0 = 7.55 \mu_B$. It is determined by the extent of demagnetization achieved during the first, nonequilibrium step, before the quasiequilibrium demagnetization sets in, and the final magnetic moment reached at the end of the process. We suppose for simplicity that the transient temperature stays constant, i.e., without heat dissipation out of the laser-excited sample volume. Moreover, Δm is assumed to depend on the sample composition due to the x -dependent T_C , and on experimental conditions like sample temperature, absorbed energy, and cooling conditions. Here Δm ranges between 0.2 and 0.3, as obtained from double exponential fits to our MOKE data according to Eq. (1). Similar values were obtained in earlier experiments [19]. We will thus use $\Delta m = 0.25$ for estimations below.

We base our estimate on a linear approximation of the concentration dependent trend in the rate of the quasiequilibrium demagnetization process $\gamma(x) = a + bx$ with $a = 0.033 \text{ ps}^{-1}$ and $b = 0.097 \text{ ps}^{-1}$, where a and b were obtained from the linear fit of $\gamma(x)$, see Fig. 3(b). We link this linear dependence to the different pathways for angular momentum transfer to the lattice by assuming $\gamma(x) = \gamma_i + \gamma_d x \alpha(x)$, where γ_d and γ_i are the rates of direct angular momentum transfer from the $4f$ shell to the lattice occurring on Tb ions, and indirect transfer through $5d$ electrons on both Tb and Gd ions, respectively [19]. The latter is supposed identical for both types of ions owing to

the similarity of ion masses and the shared $5d$ electron band of Gd and Tb, so that this contribution does not depend on the Tb content x . Since the factor $\alpha(x) = \mu_{\text{Tb}}^0/\mu_S(x)$ is close to unity, giving only a small correction to the linear dependence of γ on x , we neglect it in the following. We thus end up with $\gamma_i \approx 0.03 \text{ ps}^{-1}$ and $\gamma_d \approx 0.1 \text{ ps}^{-1}$. From this we estimate quasiequilibrium rates of angular momentum transfer to the lattice per Gd and Tb ion to $\sigma_{\text{Gd}} = \gamma_i \mu_{\text{Gd}}^0 \Delta m \approx 0.06 \mu_{\text{B}}/\text{ps}$ and $\sigma_{\text{Tb}} = (\gamma_i + \gamma_d) \mu_{\text{Tb}}^0 \Delta m \approx 0.3 \mu_{\text{B}}/\text{ps}$, respectively, which is in good agreement with our previous study [19].

So far we only considered the angular momentum transfer from the Gd and Tb ions to the lattice while implicitly assuming that both ions exhibit identical dynamics during the quasiequilibrium demagnetization, which is motivated by the results of our MOKE experiments sensitive to the element-averaged magnetization of the GdTb alloys. The angular momentum transfer to the lattice in the alloy is in this case characterized by the average transfer rate $\sigma_{\text{GdTb}} = x\sigma_{\text{Tb}} + (1-x)\sigma_{\text{Gd}}$, which is found to be $\approx 0.16 \mu_{\text{B}}/\text{ps}$ for $x = 0.4$. Such an identical dynamics of the relative magnetic moments of the Gd and Tb ions, i.e., $m_{\text{Gd}} = \mu_{\text{Gd}}/\mu_{\text{Gd}}^0$ and $m_{\text{Tb}} = \mu_{\text{Tb}}/\mu_{\text{Tb}}^0$ could be the result of $5d$ electron mediated interatomic exchange coupling between neighboring ions (RKKY coupling). However, in fact, this coupling competes with the interaction with the lattice. As shown below, the equilibration rate of Tb and Gd magnetic moments allows an estimation of the characteristic time scale of the interatomic exchange interaction. The interatomic angular momentum transfer rate via $5d$ electron mediated exchange coupling from one Gd ion to all neighboring Tb ions is, according to the values determined above, $\sigma_{\text{GdTb}}^{\text{RKKY}} = \sigma_{\text{GdTb}} - \sigma_{\text{Gd}} \approx 0.10 \mu_{\text{B}}/\text{ps}$ and correspondingly to one Tb ion from all neighboring Gd ions $\sigma_{\text{Tb}}^{\text{RKKY}} = \sigma_{\text{Tb}} - \sigma_{\text{GdTb}} \approx 0.14 \mu_{\text{B}}/\text{ps}$. Furthermore, we need to consider the number of nearest neighbors between whom angular momentum can be transferred. Thus, in the hcp lattice with coordination number $N_C = 12$ formed by $\text{Gd}_{1-x}\text{Tb}_x$, the following expressions also hold: $\sigma_{\text{Gd}}^{\text{RKKY}} = xN_C\sigma^{\text{RKKY}}$ and $\sigma_{\text{Tb}}^{\text{RKKY}} = (1-x)N_C\sigma^{\text{RKKY}}$, where σ^{RKKY} is the angular momentum transfer rate via $5d$ electron mediated interatomic exchange coupling between neighboring Gd and Tb ions. We suppose Gd and Tb in $\text{Gd}_{1-x}\text{Tb}_x$ to be identical in the considered interatomic coupling mechanism, as they share the $5d$ band. Combining the above expressions, we obtain $\sigma^{\text{RKKY}} = \Delta m[\mu_{\text{Tb}}^0\gamma_d + (\mu_{\text{Tb}}^0 - \mu_{\text{Gd}}^0)\gamma_i]/N_C \approx 0.02 \mu_{\text{B}}/\text{ps}$. This means that while assuming identical dynamics of the Gd and Tb magnetic moments, the value of the interatomic angular momentum transfer rate σ^{RKKY} is about $0.02 \mu_{\text{B}}/\text{ps}$ under the present experimental conditions. On the other hand, in the quasiequilibrium time window, the dynamics of the Gd and Tb ions cannot be absolutely identical: A difference in the relative change in magnetization of Gd and Tb will trigger a nonzero flux of angular momentum from one sublattice to another in order to obtain thermal equilibrium. In the picture discussed here, this difference originates from the stronger coupling of the Tb $4f$ magnetic moments to the lattice, so that the magnetization of the Tb sublattice is reduced faster than that of Gd. The value of this difference is as larger as stronger the coupling of Tb ions to the lattice, and as smaller as larger the maximum possible interatomic transfer rate $\sigma_{\text{max}}^{\text{RKKY}}$. Since the

latter quantity is a universal characteristic of rare earth metals, the interesting remaining question is an estimation of $\sigma_{\text{max}}^{\text{RKKY}}$.

Our time- and element-resolved XMCD measurements show that the demagnetization at the Gd and Tb ions in $\text{Gd}_{0.6}\text{Tb}_{0.4}$ is indeed identical in terms of the time scale τ_2 (compare Table I). However, in Fig. 5 one can also realize the difference $\Delta\mu/\mu_0$ in the normalized XMCD, which corresponds to a relative change of the magnetic moment, of Gd and Tb in $\text{Gd}_{0.6}\text{Tb}_{0.4}$. At 5–20 ps the demagnetization of Gd is smaller than that of Tb, and the difference increases up to $\Delta\mu/\mu_0 \approx 0.1$ at 20 ps. Subsequently, the transient difference starts to reduce and vanishes at about 40 ps (see also Fig. 5, inset), while the Tb magnetic moment is nearly constant within this interval. Consequently, the characteristic time of the process behind this transient difference can be estimated to be in the range of 5–10 ps. The magnetic moment to be transferred between neighboring Gd and Tb ions through $5d$ electron mediated interatomic exchange coupling, in order to level off their relative magnetic moments, is $\Delta\mu^{\text{RKKY}} = \mu_{\text{Tb}}^0(\frac{\Delta\mu}{\mu_0})/\{N_C[1 + x(\frac{\mu_{\text{Tb}}^0}{\mu_{\text{Gd}}^0} - 1)]\} \approx 0.07 \mu_{\text{B}}$. Estimating $\sigma_{\text{max}}^{\text{RKKY}}$ with the above characteristic time which is about 7 ps, we end up with $\sigma_{\text{max}}^{\text{RKKY}} \approx 0.01 \mu_{\text{B}}/\text{ps}$. This rough estimate is nevertheless consistent with σ^{RKKY} obtained from our MOKE experiments and can be treated as a characteristic value limiting the rate of interatomic angular momentum transfer in rare earths.

We conclude that the angular momentum transfer via interatomic exchange interaction mediated by $5d$ electrons explains the difference in Tb and Gd magnetic moments for 5–40 ps observed in Fig. 5. While an additional channel for the transfer of angular momentum from Gd to the lattice is opened via the neighboring Tb atoms, the interatomic exchange interaction acts as a bottleneck for the magnetic moment transfer between Gd and Tb and limits the loss of magnetic moment of the Gd ions to the observed value.

B. The mechanism of the demagnetization process

In finding that the first, subpicosecond time scale of demagnetization does not show a signature of a dependence on the strength of coupling of the $4f$ magnetic moments to the lattice, whereas the second demagnetization time constant clearly does, we confirm our earlier observations regarding the two-step demagnetization of rare earths [19]. Demagnetization on the subpicosecond, nonequilibrium time scale is initiated by the $5d$ electrons, but the behavior on longer time scales is dominated by the strength of direct $4f$ -lattice coupling and therefore strongly depends on the orbital anisotropy of the $4f$ shell, which defines the efficiency of angular momentum transfer to the lattice.

Regarding the initial subpicosecond demagnetization, laser-induced changes of the population of the exchange-split $5d$ band and a reduction of the exchange splitting on a similar time scale of $0.86 \pm 0.10 \text{ ps}$ have been found recently in photoemission experiments [21] (compare Table I). This is another indication that the initial demagnetization is launched by the $5d$ electrons. Since Gd and Tb in $\text{Gd}_{1-x}\text{Tb}_x$ have a shared $5d$ band, a first step in the demagnetization initiated

by the optically excited $5d$ electrons also explains why no dependence of τ_1 on the alloy composition was found.

Furthermore, the time constant of 33 ps reported here for the second demagnetization step of pure Gd is on the same order as the spin-lattice relaxation time observed [4,40] and described theoretically [41] earlier, see Table I. Consequently, a description of the ultrafast demagnetization process by equilibrium properties, in particular the Curie temperature T_C , should take the excited state into account on time scales shorter than this spin-lattice relaxation time, as thermal equilibration between the lattice and spin systems has not taken place yet.

This brings us to the question, which theoretical models potentially represent an adequate description of ultrafast magnetization dynamics in rare earths and their alloys? The microscopic three-temperature model (M3TM) [6] proposes electron-phonon spin-flip scattering of the Elliott-Yafet type as the origin of ultrafast demagnetization. It explicitly treats the case of Gd. However, the two steps observed during demagnetization are explained by the same process, namely spin flips, which occur with a certain probability at each electron-phonon scattering event [6]. In the framework of the M3TM, a two-step demagnetization is said to occur when coupling between the spin and orbital degrees of freedom is weak [42]. This is supposed to be the case for rare earths Gd and Tb, in contrast to $3d$ ferromagnets [42]. However, the very similar spin-orbit coupling constants of Gd and Tb are larger than those of the $3d$ ferromagnets [43]. This leaves differences in L as a possible cause for weak spin-lattice coupling via the spin-orbit interaction. As discussed throughout this article, spin-lattice coupling is certainly weak for Gd with an orbital moment $L = 0$. In contrast, Tb with $L = 3$ and the corresponding anisotropic $4f$ orbital configuration shows strong spin-lattice coupling, leading to increasing effective spin-lattice coupling with increasing x in $\text{Gd}_{1-x}\text{Tb}_x$, as demonstrated by our analysis of the static magnetic properties above. And yet, $\text{Gd}_{1-x}\text{Tb}_x$ shows a two-step demagnetization. Therefore, our conclusion that two different microscopic processes at the localized moment are responsible for the two steps in the ultrafast demagnetization of rare earths and their alloys suggests amendments to the M3TM [6] taking direct spin-lattice coupling of localized $4f$ magnetic moments into account. Magnetization dynamics in materials consisting of several sublattices or constituents has furthermore been described phenomenologically by atomistic modeling [44,45], which however neglects direct spin-lattice

coupling and can therefore also not be applied to Tb and its alloys [17]. Consequently, theoretical descriptions of the initial subpicosecond demagnetization [6,9,11] are to be extended to also include spin-lattice coupling and spin-orbit interaction.

IV. CONCLUSION

We have shown that combined time-resolved MOKE and XMCD measurements give information on the interactions mediating the ultrafast demagnetization process in $\text{Gd}_{1-x}\text{Tb}_x$ rare earth alloys. Concentration-dependent MOKE measurements revealed a two step demagnetization, with the time constant of the first step being independent of x , while the second reduction in magnetization was accelerated with increasing Tb content, in accordance with an increasing coupling of the $4f$ magnetic moments to the lattice via the anisotropic $4f$ orbital configuration of Tb. From element-sensitive XMCD measurements we see that the second demagnetization step occurs for Gd in $\text{Gd}_{0.6}\text{Tb}_{0.4}$ on the same time scale as for Tb, indicating an enhanced coupling of the Gd $4f$ moments to the lattice via indirect interatomic exchange (RKKY) coupling to the Tb $4f$ moments. A transient difference in the amount of demagnetization between Gd and Tb in $\text{Gd}_{0.6}\text{Tb}_{0.4}$ is attributed to a limited efficiency of this interatomic exchange coupling. We thus conclude that two different microscopic processes are responsible for the two-step demagnetization typical for rare earths Gd, Tb, and their alloys. The first, subpicosecond demagnetization is explained by the direct excitation of the $5d$ valence electrons by the pump laser, while we confirm spin-lattice coupling of the localized $4f$ magnetic moments as the driving force behind demagnetization on time scales of several picoseconds or longer.

ACKNOWLEDGMENTS

We thank Rolf Mitzner and Karsten Holldack for support during the time-resolved XMCD measurements, and the Helmholtz Zentrum Berlin for financial support for travel to BESSY II. C.S. thanks the ETH Zurich for financial support during the writing of the manuscript. Financial support by the German Ministry of Education and Research BMBF Grant 05K10PG2 FEMTOSPEX, the Deutsche Forschungsgemeinschaft through project ME3570/1, and the DAAD-HEC Pakistan is gratefully acknowledged.

-
- [1] E. Beaupaire, J.-C. Merle, A. Daunois, and J.-Y. Bigot, *Phys. Rev. Lett.* **76**, 4250 (1996).
 - [2] A. Kirilyuk, A. V. Kimel, and Th. Rasing, *Rev. Mod. Phys.* **82**, 2731 (2010).
 - [3] A. Kirilyuk, A. V. Kimel, and Th. Rasing, *Rep. Prog. Phys.* **76**, 026501 (2013).
 - [4] A. Vaterlaus, T. Beutler, and F. Meier, *Phys. Rev. Lett.* **67**, 3314 (1991).
 - [5] A. Vaterlaus, T. Beutler, D. Guarisco, M. Lutz, and F. Meier, *Phys. Rev. B* **46**, 5280 (1992).
 - [6] B. Koopmans, G. Malinowski, F. Dalla Longa, D. Steiauf, M. Fähnle, T. Roth, M. Cinchetti, and M. Aeschlimann, *Nat. Mater.* **9**, 259 (2009).
 - [7] E. Carpena, E. Mancini, C. Dallera, M. Brenna, E. Puppini, and S. De Silvestri, *Phys. Rev. B* **78**, 174422 (2008).
 - [8] M. Krauß, T. Roth, S. Alebrand, D. Steil, M. Cinchetti, M. Aeschlimann, and H. C. Schneider, *Phys. Rev. B* **80**, 180407(R) (2009).
 - [9] B. Y. Mueller, A. Baral, S. Vollmar, M. Cinchetti, M. Aeschlimann, H. C. Schneider, and B. Rethfeld, *Phys. Rev. Lett.* **111**, 167204 (2013).
 - [10] A. B. Schmidt, M. Pickel, M. Donath, P. Buczek, A. Ernst, V. P. Zhukov, P. M. Echenique, L. M. Sandratskii, E. V. Chulkov, and M. Weinelt, *Phys. Rev. Lett.* **105**, 197401 (2010).
 - [11] M. Battiato, K. Carva, and P. M. Oppeneer, *Phys. Rev. Lett.* **105**, 027203 (2010).

- [12] A. Melnikov, I. Razdolski, T. O. Wehling, E. Th. Papaioannou, V. Roddatis, P. Fumagalli, O. Aktsipetrov, A. I. Lichtenstein, and U. Bovensiepen, *Phys. Rev. Lett.* **107**, 076601 (2011).
- [13] D. Rudolf *et al.*, *Nat. Commun.* **3**, 1037 (2011).
- [14] A. Eschenlohr, M. Battiato, P. Maldonado, N. Pontius, T. Kachel, K. Holldack, R. Mitzner, A. Föhlisch, P. M. Oppeneer, and C. Stamm, *Nat. Mater.* **12**, 332 (2013).
- [15] E. Turgut *et al.*, *Phys. Rev. Lett.* **110**, 197201 (2013).
- [16] I. Radu *et al.*, *Nature (London)* **472**, 205 (2011).
- [17] A. R. Khorsand, M. Savoini, A. Kirilyuk, A. V. Kimel, A. Tsukamoto, A. Itoh, and Th. Rasing, *Phys. Rev. Lett.* **110**, 107205 (2013).
- [18] S. Mathias *et al.*, *Proc. Natl. Acad. Sci. U.S.A.* **109**, 4792 (2012).
- [19] M. Wietstruk, A. Melnikov, C. Stamm, T. Kachel, N. Pontius, M. Sultan, C. Gahl, M. Weinelt, H. A. Dürr, and U. Bovensiepen, *Phys. Rev. Lett.* **106**, 127401 (2011).
- [20] U. Bovensiepen, *J. Phys.: Condens. Matter* **19**, 083201 (2007).
- [21] R. Carley, K. Döbrich, B. Frietsch, C. Gahl, M. Teichmann, O. Schwarzkopf, P. Wernet, and M. Weinelt, *Phys. Rev. Lett.* **109**, 057401 (2012).
- [22] This difference in spin-lattice coupling is responsible for a two orders of magnitude difference in the magnetoelastic constants of Gd and Tb, see B. Coqblin, *The Electronic Structure of Rare-Earth Metals and Alloys* (Academic, London, 1977).
- [23] D. M. S. Bagguley, J. P. Partington, J. A. Robertson, and R. C. Woods, *J. Phys. F: Met. Phys* **10**, 967 (1980).
- [24] M. Wietstruk, Ph.D. thesis, Technische Universität, Berlin, 2010.
- [25] M. Colarieti-Tosti, S. I. Simak, R. Ahuja, L. Nordström, O. Eriksson, D. Åberg, S. Edvardsson, and M. S. S. Brooks, *Phys. Rev. Lett.* **91**, 157201 (2003).
- [26] K. Tajima, *J. Phys. Soc. Jpn.* **31**, 441 (1971).
- [27] K. Starke, F. Heigl, A. Vollmer, M. Weiss, G. Reichardt, and G. Kaindl, *Phys. Rev. Lett.* **86**, 3415 (2001).
- [28] M. Sultan, A. Melnikov, and U. Bovensiepen, *Phys. Status Solidi B* **248**, 2323 (2011).
- [29] M. Sultan, U. Atxitia, A. Melnikov, O. Chubykalo-Fesenko, and U. Bovensiepen, *Phys. Rev. B* **85**, 184407 (2012).
- [30] J. Stöhr, *J. Electron. Spectrosc. Relat. Phenom.* **75**, 253 (1995).
- [31] Please note that the different film thicknesses and substrates for the samples used in our MOKE and XMCD studies do not affect the magnetization dynamics on time scales less than ≈ 50 ps. Only the time needed for recovery of the magnetic signal back to its value before laser excitation is longer in the XMCD samples on freestanding membranes, due to a less effective heat transfer out of the excited region, see M. Sultan, Ph.D. thesis, Freie Universität, Berlin, 2012.
- [32] C. T. Chen, Y. U. Idzerda, H.-J. Lin, N. V. Smith, G. Meigs, E. Chaban, G. H. Ho, E. Pellegrin, and F. Sette, *Phys. Rev. Lett.* **75**, 152 (1995).
- [33] A. Berger, A. W. Pang, and H. Hopster, *J. Magn. Magn. Mater.* **137**, L1 (1994).
- [34] S. Khan, K. Holldack, T. Kachel, R. Mitzner, and T. Quast, *Phys. Rev. Lett.* **97**, 074801 (2006).
- [35] C. Stamm *et al.*, *Nat. Mater.* **6**, 740 (2007).
- [36] J. Feikes, K. Holldack, P. Kuske, and G. Wüstefeld, *Proceedings of EPAC* (European Physical Society Accelerators Group at CERN, Geneva, Switzerland, 2004), p. 1954.
- [37] The time constant τ_2 for Gd and Tb in $\text{Gd}_{0.6}\text{Tb}_{0.4}$ is potentially somewhat shorter than the τ_2 derived for pure Tb in [19] because we could not take the recovery of the magnetic signal to its equilibrium value before laser excitation into account in fitting the present dataset, in contrast to [19].
- [38] A systematic error in the measurement is excluded: During the experiment we frequently alternated between measurements at the Gd and Tb M_5 edges to ensure that potential drifts in the temporal or spatial pump-probe overlap affect both measurements equally.
- [39] L. Zhang and Q. Niu, *Phys. Rev. Lett.* **112**, 085503 (2014).
- [40] A. Melnikov, H. Prima-Garcia, M. Lisowski, T. Gießel, R. Weber, R. Schmidt, C. Gahl, N. M. Bulgakova, U. Bovensiepen, and M. Weinelt, *Phys. Rev. Lett.* **100**, 107202 (2008).
- [41] W. Hübner and K. H. Bennemann, *Phys. Rev. B* **53**, 3422 (1996).
- [42] T. Roth, A. J. Schellekens, S. Alebrand, O. Schmitt, D. Steil, B. Koopmans, M. Cinchetti, and M. Aeschlimann, *Phys. Rev. X* **2**, 021006 (2012).
- [43] J. Stöhr and H. C. Siegmann, *Magnetism: From Fundamentals to Nanoscale Dynamics* (Springer, Berlin, 2006).
- [44] T. A. Ostler *et al.*, *Nat. Commun.* **3**, 666 (2012).
- [45] J. H. Mentink, J. Hellsvik, D. V. Afanasiev, B. A. Ivanov, A. Kirilyuk, A. V. Kimel, O. Eriksson, M. I. Katsnelson, and Th. Rasing, *Phys. Rev. Lett.* **108**, 057202 (2012).